



Preparation and characterization of $\text{La}_{1.75}\text{Y}_{0.25}\text{Mo}_{2-x}\text{Al}_x\text{O}_{9-\delta}$ as solid electrolyte for intermediate temperatures SOFC

Changan Tian¹, Minzheng Zhu^{1,2}, Lingbo Shao², Xiaoling Qu¹, Lejie Zhu^{1,*}, Chao Chen¹, Cao Wang¹, Yang Liu^{1,*}

¹College of Chemistry and Civil Engineering, Shaoguan University, Shaoguan 512005, China

²College of Energy Material and Chemical Engineering, Hefei University, Hefei 230601, China

Received 12 June 2022; Received in revised form 29 September 2022; Received in revised form 14 December 2022;

Accepted 4 January 2023

Abstract

Yttrium and aluminium co-substitutions on lanthanum molybdate ceramics with the nominal formula $\text{La}_{1.75}\text{Y}_{0.25}\text{Mo}_{2-x}\text{Al}_x\text{O}_{9-\delta}$ (LYMA, $x = 0, 0.1, 0.2, 0.3$ and 0.4) were synthesized by citric acid-nitrate combustion method and used for preparation of solid electrolyte for intermediate-temperature solid oxide fuel cells (IT-SOFCs). Phase composition, structure, conductivity and electrical properties of LYMA have been investigated as a function of aluminium content by X-ray diffraction, scanning electron microscopy and electrochemical impedance spectroscopy, respectively. Experimental results showed that the substitution of La and Mo with appropriate amounts of Y and Al can effectively stabilize the β -form of $\text{La}_2\text{Mo}_2\text{O}_9$ at room temperature and inhibit its phase transition to α -form. The LYMA synthesized by combustion method exhibited a better sinterability where relative density of the samples sintered at 950°C for 4 h was higher than 95 %TD. The performance of the LYMA electrolyte was found to be related to Al-content. The $\text{La}_{1.75}\text{Y}_{0.25}\text{Mo}_{1.8}\text{Al}_{0.2}\text{O}_{8.7}$ exhibited high oxide ion conductivity ($\sigma = 42 \text{ mS/cm}$ at 800°C) and low electrical activation energy ($E_a = 1.18 \text{ eV}$). These preliminary results indicate that the LYMA is a promising electrolyte for IT-SOFCs.

Keywords: SOFCs, electrolyte, $\text{La}_2\text{Mo}_2\text{O}_9$, combustion method, conductivity

I. Introduction

Solid oxide fuel cells (SOFCs) have attracted great attention because of their high energy-conversion efficiency, low pollution and good fuel flexibility [1–3]. SOFCs mainly consist of electrolyte, cathode and anode materials. Among these, the electrolyte is the most important component as it acts as a membrane, transporting ionic oxygen from cathode to anode side. Therefore the electrolyte should have fast ionic transport, negligible electronic conduction and stability at the operating temperature [1–6]. Yttria-stabilized zirconia (YSZ) is a well-known electrolyte for SOFCs, which requires operating temperature above 800°C . However, the high working temperature leads to a series of problems such as interfacial reaction between the compo-

nents, mechanical and thermal degradation, thermal expansion, mismatch and high cost of materials. Therefore, a major challenge in reducing the operating temperature of SOFCs is to develop alternative electrolyte materials that can operate at intermediate-temperatures ($500\text{--}800^\circ\text{C}$) with high oxygen-ion conductivity [7–12].

In recent years, $\text{La}_2\text{Mo}_2\text{O}_9$ based ceramics (LAMO) have been regarded as a candidate for electrolyte material, because of high ionic conductivity ($\sim 10^{-2} \text{ S cm}^{-1}$) of the parent compound at 800°C which is comparable to the conductivity of YSZ at 1000°C [11–16]. However, it is noteworthy that $\text{La}_2\text{Mo}_2\text{O}_9$ has two polymorphs, a low-temperature monoclinic α -phase ($P2_1$) and a high temperature cubic β -phase ($P2_13$), with a first-order phase transition around 580°C . $\text{La}_2\text{Mo}_2\text{O}_9$ exhibits high ionic conductivity only in cubic phase (β) at a temperature higher than 580°C . $\text{La}_2\text{Mo}_2\text{O}_9$ conductivity reduces approximately two orders of magnitude below 580°C due to the phase transition from cubic structured high-temperature conduc-

*Corresponding author: tel: +86 751 8120156

e-mail: tca2204@126.com (Lejie Zhu)

liuyang1987@sgu.edu.cn (Yang Liu)

tive β phase to monoclinic structured low-temperature α phase. The $\alpha \leftrightarrow \beta$ phase transition is also causing abrupt volume change. On the other hand, the readily occurring reduction of Mo^{6+} to Mo^{4+} under reducing conditions causes mixed ionic-electronic conduction and also promoting LAMOX degradation [12,15–17]. Substitutions have been done to suppress the monoclinic (α) to cubic (β) phase transition of the parent compound that occurs at around 580 °C and furthermore to overcome the reduction issue of Mo^{6+} at low oxygen partial pressures. At La site of $\text{La}_2\text{Mo}_2\text{O}_9$, various dopants, like Y^{3+} , K^+ , Rb^+ , Ca^{2+} , Ba^{2+} , Sr^{2+} , Dy^{3+} , Er^{3+} , Sm^{3+} , Bi^{3+} , etc. have been reported to be effective in the stabilization of β -polymorph at room temperature and in the increase the ionic conductivity. But the long-term stability of LAMOX is still questionable as the Mo^{6+} is very much prone to reduction under reducing atmosphere [11,12,18,19]. Al^{3+} , V^{5+} , W^{6+} , Cr^{6+} , Nb^{5+} , Ga^{6+} , etc. substitution on Mo sites have exhibited enhancement in the stabilization of $\text{La}_2\text{Mo}_2\text{O}_9$ in reducing atmosphere. By considering the advantages and disadvantages of the substitution effect on La and Mo sites, double substitutions offer the opportunity to improve the stability of $\text{La}_2\text{Mo}_2\text{O}_9$ by suppressing the phase transition and improving ionic conductivity [11,12,18–20]. Therefore, Y and Al co-substituted $\text{La}_2\text{Mo}_2\text{O}_9$ could be possibly used as SOFCs electrolytes in the intermediate temperature range and under moderate reducing conditions.

Nanopowders provide sufficient densification at the lower sintering temperature, good mechanical properties and enhance electrical properties. Ultrafine nanopowder of LAMOX has been reported to be synthesized by various wet chemical routes, such as freeze-drying precursors, high power ball milling, EDTA complexing method, combustion method, etc. [12,17,21–23]. Among the above-mentioned processes the solution combustion process is characterized by fast reaction rate and low cost. In the solution combustion route a self-sustaining exothermic redox reaction is allowed to take place in the gel that is formed upon dehydrating an aqueous solution of a fuel (such as citric acid) and an oxidant (metal nitrate).

In the presented work, La and Mo were substituted with Y and Al in order to suppress the thermal activation order-disorder phase transition and stabilize the β phase in $\text{La}_2\text{Mo}_2\text{O}_9$ at lower temperature. Oxides with nominal composition of $\text{La}_{1.75}\text{Y}_{0.25}\text{Mo}_{2-x}\text{Al}_x\text{O}_{9-\delta}$ (LYMA, $x = 0, 0.1, 0.2, 0.3$ and 0.4) were synthesized by citric acid-nitrate combustion method. The effects of x on the crystal structure, morphology, ionic conductivity and electrochemical performance were systematically investigated.

II. Experimental

2.1. Sample preparation

The $\text{La}_{1.75}\text{Y}_{0.25}\text{Mo}_{2-x}\text{Al}_x\text{O}_{9-\delta}$ (LYMA, $x = 0, 0.1, 0.2, 0.3$ and 0.4) materials were synthesized via the citric acid-nitrate combustion method. All

raw materials, $\text{La}(\text{NO}_3)_3 \cdot 6\text{H}_2\text{O}$, $\text{Y}(\text{NO}_3)_3 \cdot 6\text{H}_2\text{O}$, $(\text{NH}_4)_6\text{Mo}_7\text{O}_{24} \cdot 4\text{H}_2\text{O}$ and $\text{Al}(\text{NO}_3)_3 \cdot 9\text{H}_2\text{O}$, were from Shanghai Aladdin Biochemical Technology Co. Ltd. and the purity was higher than 99.0% (AR). At first, stoichiometric amounts of precursors were dissolved in deionized water in a glass beaker and allowed to stir on a hot plate for 0.5 h to get a homogenized mixture of metal ions. Then the corresponding mass of citric acid was added in a molar ratio of citric acid : metal cations = 2 : 1, in order to chelate cations. In order to promote the complexation of the metal ions, the pH was adjusted to around 7 by slow addition of ammonia solution. The mixture was heated under stirring at 80 °C for 12 h forming a transparent and viscous gel. On further heating, the temperature of the gel increased and an auto-combustion of the gel took place with production of large amount of gas. The as-synthesized powder was then calcined at 600 °C for 2 h to remove the residual organic species and get the final powders. The calcined powders were reground and pressed into pellets (diameter 10 mm and thickness ~ 1.0 mm) by uniaxial pressing under 120 MPa. The pellets were sintered at 950 °C for 4 h with a heating rate of 5 °C/min and cooling rate of 3 °C/min.

2.2. Characterization

Fourier transform infrared (FTIR) spectra of the samples were obtained on a FTIR analyser (Model 8400S, Japan) in the wavenumber range of 400–4000 cm^{-1} . The xerogels were studied by simultaneous thermogravimetric (TG) and differential scanning calorimetry (DSC) (Model Netzsch STA 409PC, Germany) in the temperature range of room temperature to 700 °C under a flow of air with a heating rate of 10 °C/min. The crystal phase structure of the synthesized powders was gauged by X-ray diffraction (XRD, Model Rigaku) with a 2θ range of 10–70°, a scanning rate of 5 °/min, and a $\text{Cu K}\alpha$ radiation source ($\lambda = 0.15406$ nm). The surface morphology of the electrolyte was inspected by scanning electron microscopy (SEM, Model SU8220). For conductivity measurements, silver contacts were applied on both the sintered sample surfaces and cured at 700 °C for 10 min. An impedance analyser (Model Solartron SI-1260, England) was used to measure the impedance spectra in frequency range from 20 Hz to 5 MHz and temperatures from 400 to 800 °C in air. To determine the ionic conductivity of electrolytes, the impedance data were fitted to equivalent electronic circuit using ZSimpWin software.

III. Results and discussion

3.1. FTIR and thermal analysis

FTIR spectra of the $\text{La}_{1.75}\text{Y}_{0.25}\text{Mo}_{2-x}\text{Al}_x\text{O}_{9-\delta}$ xerogels are shown in Fig. 1. It shows that there are few bands in the range from 400 to 4000 cm^{-1} and the bands were attributed to the various functional groups. The peaks around 3741, 2314 and 1681 cm^{-1} could correspond to

O–H stretching, –OC and COO– antisymmetric stretching, respectively [24–26]. The peak at 1519 cm^{-1} possibly arises due to the stretching vibrations of the NO_3^- ion, demonstrating that NO_3^- is involved in formation of the colloid [27]. Peaks observed at wavenumbers 964 and 521 cm^{-1} are ascribed to the characteristic stretching of metal-oxygen bonds, supporting the presence of citrate metal chelate species [28].

TG-DSC curves of the $\text{La}_{1.75}\text{Y}_{0.25}\text{Mo}_{2-x}\text{Al}_x\text{O}_{9-\delta}$ xerogel are presented in Fig. 2. They showed that the xerogel decomposes in the following three stages: dehydration, decomposition of the citrate and oxidation of the decomposition products. A small weight loss from room temperature to about 150°C is due to desorption of physisorbed water. In the DSC curve, the first exothermic peak at 215°C reveals the combustion of organic species. The second exothermic peak at 285°C corresponds to the residual organic matter. As the TG curve shows, the weight of the sample decreases significantly between 190 and 400°C and no remarkable change can be seen in the DSC curve above 400°C . This proves that the $\text{La}_{1.75}\text{Y}_{0.25}\text{Mo}_{1.8}\text{Al}_{0.2}\text{O}_{8.7}$ has been almost perfectly crystallized beyond this temperature. But, the slight weight losses can be found above 400°C in the TG curve, which are due to the oxidation of re-

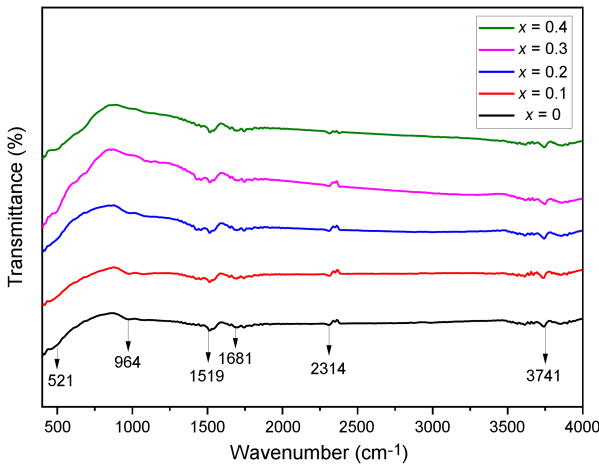


Figure 1. FTIR spectra of $\text{La}_{1.75}\text{Y}_{0.25}\text{Mo}_{2-x}\text{Al}_x\text{O}_{9-\delta}$ xerogels

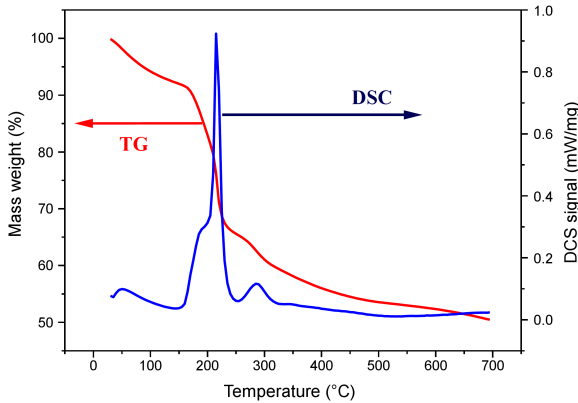


Figure 2. TG-DSC curve of $\text{La}_{1.75}\text{Y}_{0.25}\text{Mo}_{1.8}\text{Al}_{0.2}\text{O}_{8.7}$ xerogel

maining carbonaceous material. Based on the TG-DSC results the powders synthesized by combustion route were calcined at 600°C .

3.2. Crystal structure and particle size analysis

Figure 3 shows XRD patterns of the $\text{La}_{1.75}\text{Y}_{0.25}\text{Mo}_{2-x}\text{Al}_x\text{O}_{9-\delta}$ ($x = 0, 0.1, 0.2, 0.3$ and 0.4) calcined at 600°C for 2 h. The XRD patterns confirm that the compositions having $x = 0$ and $x = 0.1$ exhibit a single cubic phase (JCPDS Card No. 28-0509). The formation of a single phase clearly indicates that Y and Al cations were successfully introduced into the La and Mo sites, separately. The sample can be indexed as the cubic system, space group $P2_13$ having the β structure. XRD patterns of the samples with $x \geq 0.2$ reveal the presence of secondary phases. These suggest that the solubility limit of Al in $\text{La}_2\text{Mo}_2\text{O}_9$ is no more than 20%. The solubility of Al in $\text{La}_2\text{Mo}_2\text{O}_9$ is limited because of the different ion size and crystal structures, which leads to the generation of other phases [29]. From Table 1, the cell lattice parameter of the $\text{La}_{1.75}\text{Y}_{0.25}\text{Mo}_{2-x}\text{Al}_x\text{O}_{9-\delta}$ (calculated from the XRD patterns in Fig. 3) changes with Al content (x), and decreases from 7.1517 to 7.1477 \AA with x increasing from 0 to 0.2, because the radius of Al^{3+} (0.0535 nm) is smaller than Mo^{6+} (0.065 nm). However, as x increases further from 0.2 to 0.4, the lattice parameter increases from 7.1477 to 7.1582 \AA . The slight increase in the cell parameter for the $x > 0.2$ compositions may be linked with the formation of excess Al^{3+} in these cases [29].

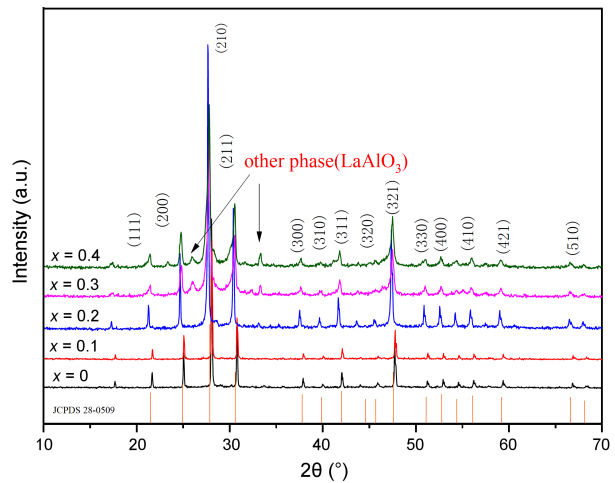


Figure 3. XRD patterns of $\text{La}_{1.75}\text{Y}_{0.25}\text{Mo}_{2-x}\text{Al}_x\text{O}_{9-\delta}$ powders

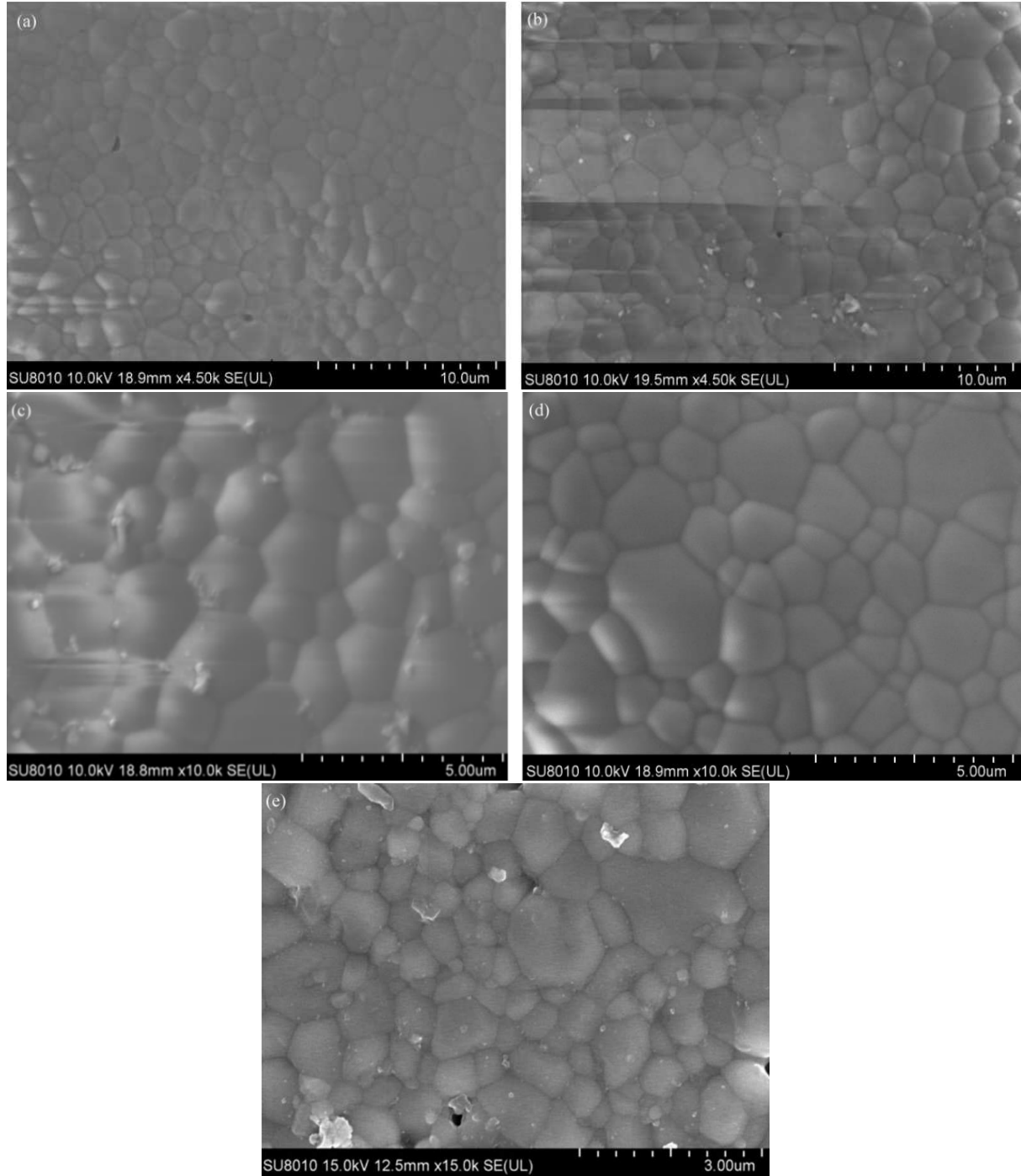
The average crystallite size of the sample was calculated by using the Debye-Scherrer equation:

$$D = \frac{0.9 \cdot \lambda}{\beta \cdot \cos \theta} \quad (1)$$

where D is the crystallite size in nm, λ is the radiation wave length (for Cu K_α $\lambda = 0.15406\text{ nm}$), β is full width at half height of the strongest Bragg's peak corresponding to (210) reflection of the samples, θ is the corre-

Table 1. Lattice parameter and crystallite size of $\text{La}_{1.75}\text{Y}_{0.25}\text{Mo}_{2-x}\text{Al}_x\text{O}_{9-\delta}$ ($0 \leq x \leq 0.4$) powders and properties of ceramics

x [mol]	Lattice parameter, a [Å]	Average crystallite size, D [nm]	Relative density [%TD]	Electrical conductivity, $\sigma_{800^\circ\text{C}}$ [mS/cm]	Activation energy, E_a [eV]
0	7.1517	62	96.5	2.4	1.47
0.1	7.1509	61	96.9	28	1.26
0.2	7.1477	54	98.3	42	1.18
0.3	7.1479	46	97.4	30	1.59
0.4	7.1582	43	95.2	25	1.61

**Figure 4. Images of $\text{La}_{1.75}\text{Y}_{0.25}\text{Mo}_{2-x}\text{Al}_x\text{O}_{9-\delta}$ SEM. (a) $x = 0$; (b) $x = 0.1$; (c) $x = 0.2$; (d) $x = 0.3$; (e) $x = 0.4$**

sponding peak diffraction angle. The average crystallite size values of the $\text{La}_{1.75}\text{Y}_{0.25}\text{Mo}_{2-x}\text{Al}_x\text{O}_{9-\delta}$ nanopowders at various compositions are given in Table 1. The

crystallite sizes of the $\text{La}_{1.75}\text{Y}_{0.25}\text{Mo}_{2-x}\text{Al}_x\text{O}_{9-\delta}$ powders calcined at 600°C for 2 h, calculated by the Debye-Scherrer equation, were between 43 and 62 nm. Thus,

ultrafine $\text{La}_{1.75}\text{Y}_{0.25}\text{Mo}_{2-x}\text{Al}_x\text{O}_{9-\delta}$ powders with cubic phase (β) structure were successfully prepared after calcination at 600°C for 2 h, further demonstrating that the citric acid-nitrate combustion method permits the use of a lower temperature for the synthesis of the $\text{La}_{1.75}\text{Y}_{0.25}\text{Mo}_{2-x}\text{Al}_x\text{O}_{9-\delta}$ powders.

3.3. Sinterability and microstructure

A dense electrolyte is needed in SOFCs to prevent gas mixing and transport of oxygen ion. Relative density of the $\text{La}_{1.75}\text{Y}_{0.25}\text{Mo}_{2-x}\text{Al}_x\text{O}_{9-\delta}$ sintered in air at 950°C for 4 h was measured by the Archimedes' principle and shown in Table 1. It can be seen that the relative density of the samples increases with x and then decreases. The highest relative density (98.3 %TD) was reached for the ceramics with $x = 0.2$. Also, the measured density of all samples is greater than 95 %TD, while other kinds of solid electrolytes often require sintering temperature over 1000°C in order to obtain this density [1–3,7,9]. The density results demonstrate the high sintering activity of the $\text{La}_{1.75}\text{Y}_{0.25}\text{Mo}_{2-x}\text{Al}_x\text{O}_{9-\delta}$ powders prepared by citric acid-nitrate combustion method. As shown in Fig. 4 the cross-sectional SEM images of the $\text{La}_{1.75}\text{Y}_{0.25}\text{Mo}_{2-x}\text{Al}_x\text{O}_{9-\delta}$ sintered at 950°C for 4 h reveal that the surface has a good densification with very few small pores and that average grain size is $2\mu\text{m}$. This may be assumed to be the reason for the high conductivity of the sample. The electrolyte with

larger grain size is therefore expected to yield better cell performance, since grain boundaries induce space charge layer decrease thus increasing ionic conductivity [30]. Therefore, it can be said that the citric acid-nitrate combustion method is a facile route to synthesize $\text{La}_{1.75}\text{Y}_{0.25}\text{Mo}_{2-x}\text{Al}_x\text{O}_{9-\delta}$ materials for SOFCs applications.

3.4. Electrical characterization

Figure 5 shows the AC impedance diagram of the $\text{La}_{1.75}\text{Y}_{0.25}\text{Mo}_{1.8}\text{Al}_{0.2}\text{O}_{8.7}$ sintered at 950°C for 4 h. It can be seen that the impedance spectrum consists of a semicircle and a arc. The semicircle corresponds to the overlapping of grain and grain boundary impedance contribution, the arc corresponds to ionic and electronic conduction of the electrode [1,31]. Grain resistance (R_g) and grain boundary resistance (R_{gb}) were distinguished using the ZSimpWin software by modelling the impedance spectrum with the equivalent circuit.

Total resistance (R_t) of the sample was the sum of R_b and R_{gb} . Total ionic conductivity (σ_t) at different temperatures was determined using the following equation [32]:

$$\sigma_t = \frac{D}{S \cdot R_t} \quad (2)$$

where D , S and R_t represent the thickness, area and resistance of the sample, respectively.

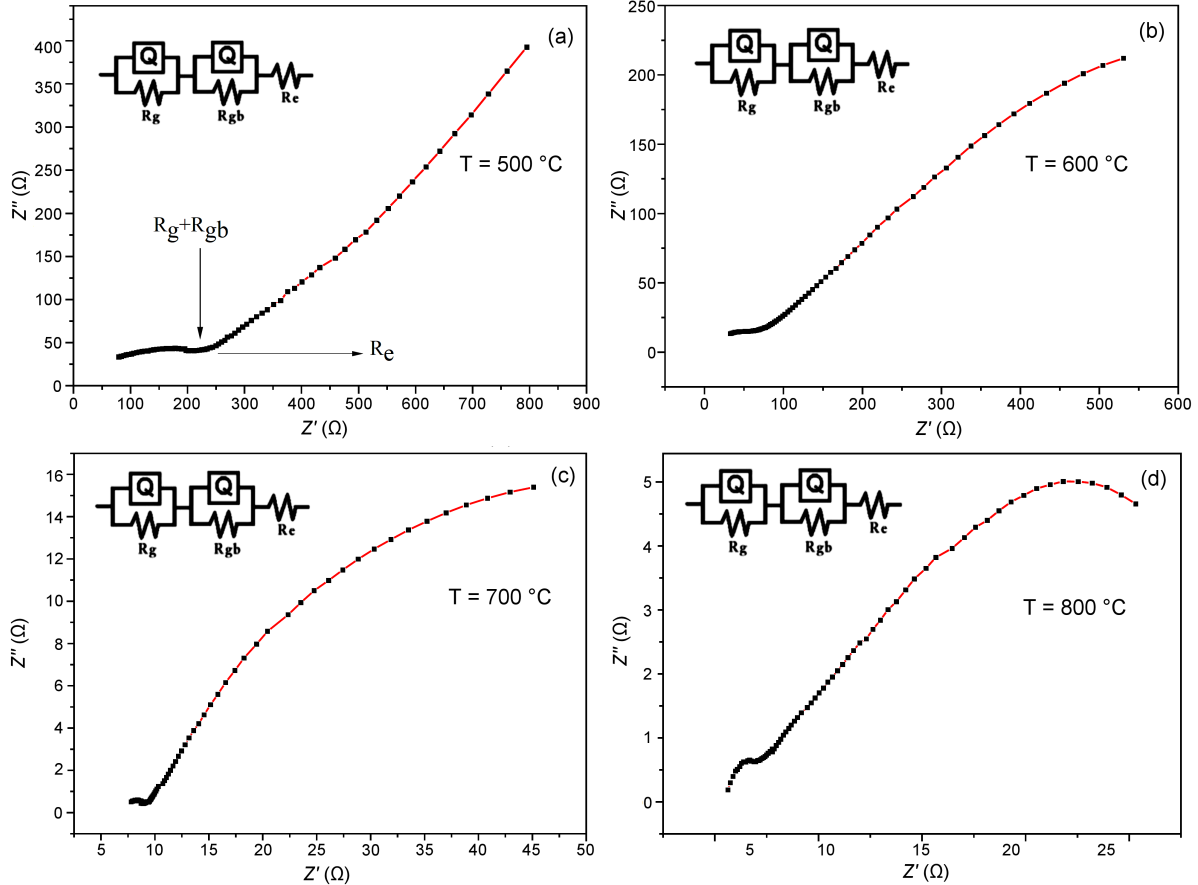


Figure 5. AC impedance diagrams of $\text{La}_{1.75}\text{Y}_{0.25}\text{Mo}_{1.8}\text{Al}_{0.2}\text{O}_{8.7}$ at: a) 500°C , b) 600°C , c) 700°C and d) 800°C

Figure 6 shows the temperature dependence of total ionic conductivity of the $\text{La}_{1.75}\text{Y}_{0.25}\text{Mo}_{2-x}\text{Al}_x\text{O}_{9-\delta}$. As it can be seen from Fig. 6, ionic conductivity of the system improves on doping with Al, and conductivity of the samples abruptly increases from 2.4 mS/cm to a maximum of 42 mS/cm at 800 °C, with x increasing from 0 to 0.2. However, as x further increase, conductivity falls and drops to 25 mS/cm at $x = 0.4$. In addition, conductivity for the $\text{La}_{1.75}\text{Y}_{0.25}\text{Mo}_{2-x}\text{Al}_x\text{O}_{9-\delta}$ is nearly independent of the oxygen partial pressure between 0.21 and 10^{-5} atm at 1073 K, which indicated that within the oxygen partial pressure range the conductivity was predominantly oxygen ionic in nature [11,17,33]. The conductivity values of the $\text{La}_{1.75}\text{Y}_{0.25}\text{Mo}_{2-x}\text{Al}_x\text{O}_{9-\delta}$ are comparable to the data already published in the literature (Table 2). Based on the electrical measurements at an intermediate temperature, we present these materials for future use in SOFCs. This study also suggested that Y and Al co-doping could enhance the electrical properties of the $\text{La}_2\text{Mo}_2\text{O}_9$ based electrolyte.

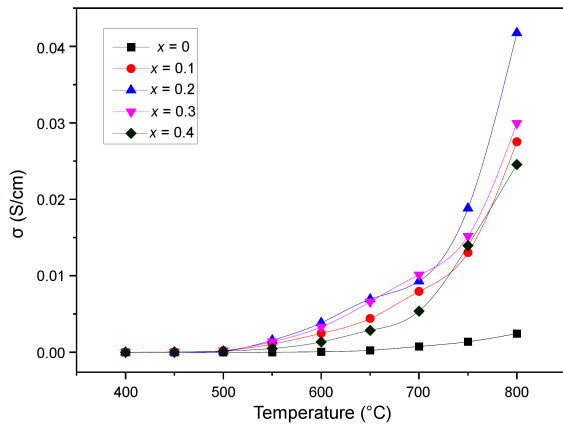


Figure 6. Conductivity of the samples in air at different x

Table 2. Conductivity of some important materials

Material	Conductivity	Ref.
YSZ	25 mS/cm at 1000 °C	[19]
$\text{La}_2\text{Mo}_{1.7}\text{W}_{0.3}\text{O}_{9-\delta}$	60.4 mS/cm at 800 °C	[34]
$\text{La}_2\text{Mo}_{1.95}\text{V}_{0.05}\text{O}_{9-\delta}$	34.6 mS/cm at 750 °C	[32]
$\text{La}_2\text{Mo}_{1.97}\text{Sn}_{0.03}\text{O}_{9-\delta}$	55 mS/cm at 800 °C	[35]
$\text{La}_{1.7}\text{Dy}_{0.3}\text{Mo}_{1.7}\text{W}_{0.3}\text{O}_9$	10.5 mS/cm at 800 °C	[18]
$\text{La}_{1.9}\text{Ba}_{0.1}\text{Mo}_{1.85}\text{W}_{0.15}\text{O}_{8.95}$	30.7 mS/cm at 800 °C	[15]
$\text{Ce}_{0.95}\text{Gd}_{0.05}\text{O}_{2-\delta}$	10.5 mS/cm at 800 °C	[36]

Figure 7 shows the Arrhenius plot of total conductivity of the $\text{La}_{1.75}\text{Y}_{0.25}\text{Mo}_{2-x}\text{Al}_x\text{O}_{9-\delta}$ electrolyte. The total conductivity data were well fitted with straight lines throughout the operating temperatures, indicating that conductivity of the $\text{La}_{1.75}\text{Y}_{0.25}\text{Mo}_{2-x}\text{Al}_x\text{O}_{9-\delta}$ obeys the Arrhenius law in the test temperature range. It is showed that no phase transition has happened in the investigated temperature range which further illustrates that Al and Y co-doping could suppress the first-order phase transformation of $\text{La}_2\text{Mo}_2\text{O}_9$ and stabilize the cubic structure at room temperature [15,37].

The temperature dependence of total conductivity of the $\text{La}_{1.75}\text{Y}_{0.25}\text{Mo}_{2-x}\text{Al}_x\text{O}_{9-\delta}$ electrolyte can be expressed by the Arrhenius equation [32]:

$$\sigma_t = \frac{\sigma_0}{T} \exp\left(-\frac{E_a}{k \cdot T}\right) \quad (3)$$

where σ_0 , E_a , k and T are the pre-exponential factor, activation energy, Boltzmann constant and absolute temperature, respectively. Figure 8 shows the variation of activation energy as a function of Al dopant concentration in the $\text{La}_{1.75}\text{Y}_{0.25}\text{Mo}_{2-x}\text{Al}_x\text{O}_{9-\delta}$. The activation energies are 1.47 eV ($x = 0.0$), 1.26 eV ($x = 0.1$), 1.18 eV ($x = 0.2$), 1.59 eV ($x = 0.3$) and 1.61 eV ($x = 0.4$). The enhanced Al^{3+} concentration causes the generation of oxygen vacancies and minimizes the association energy between dopant cations and oxygen vacancies leading to the high oxygen ion conductivity. From Table 1 it can be clearly seen that the composition $\text{La}_{1.75}\text{Y}_{0.25}\text{Mo}_{1.8}\text{Al}_{0.2}\text{O}_{8.7}$ has the highest conductivity and the minimal activation energy, which is because of interaction amongst the dopant-cations and mobile oxygen vacancies within the $\text{La}_2\text{Mo}_2\text{O}_9$ lattice. The elec-

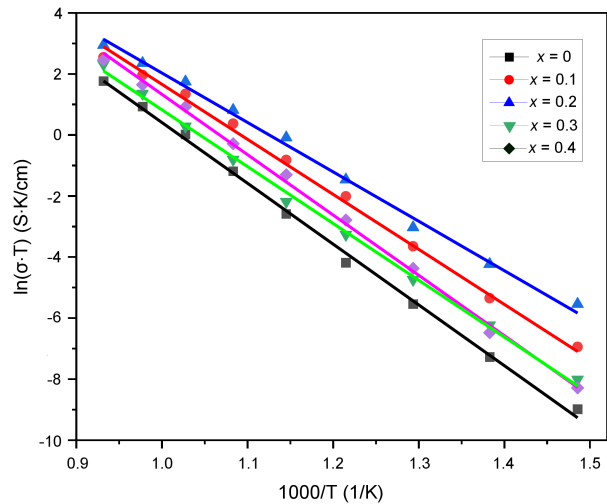


Figure 7. The Arrhenius curves for $\text{La}_{1.75}\text{Y}_{0.25}\text{Mo}_{2-x}\text{Al}_x\text{O}_{9-\delta}$

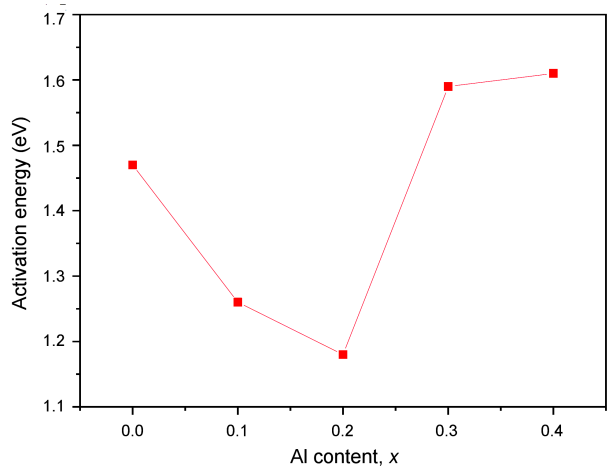


Figure 8. Activation energy for $\text{La}_{1.75}\text{Y}_{0.25}\text{Mo}_{2-x}\text{Al}_x\text{O}_{9-\delta}$

trochemical results reported in this work show the efficiency of the citric acid-nitrate combustion process for the low temperature preparation of Y and Al co-doped $\text{La}_2\text{Mo}_2\text{O}_9$ ceramics as candidates to be used as electrolytes in SOFCs applications.

IV. Conclusions

Electrolyte $\text{La}_{1.75}\text{Y}_{0.25}\text{Mo}_{2-x}\text{Al}_x\text{O}_{9-\delta}$ ($x = 0, 0.1, 0.2, 0.3, 0.4$) materials were prepared by citric acid-nitrate combustion reaction. XRD results indicated that single cubic β -phase was successfully obtained after calcination at 600°C for 2 h and the solubility limit of Al in $\text{La}_2\text{Mo}_2\text{O}_9$ is no more than 20%. The $\text{La}_{1.75}\text{Y}_{0.25}\text{Mo}_{2-x}\text{Al}_x\text{O}_{9-\delta}$ powders synthesized by combustion reaction had very good sinterability and relative density of all samples sintered at 950°C for 4 h was more than 95 %TD. The impedance spectroscopy results indicated that the Y and Al doped $\text{La}_2\text{Mo}_2\text{O}_9$ can improve ionic conductivity. Moreover, Y and Al co-doping suppress the phase transition and effectively stabilize the β phase at low temperature. Among all compositions, the $\text{La}_{1.75}\text{Y}_{0.25}\text{Mo}_{1.8}\text{Al}_{0.2}\text{O}_{8.7}$ shows the highest conductivity of 42 mS/cm at 800°C and minimal activation energy of 1.18 eV, which can be a promising electrolyte material for IT-SOFCs.

Acknowledgment: This work was supported by the Guangdong Basic and Applied Basic Research Foundation (No. 2021A1515010671, 2020A1515011221) and the Guangdong Province Key Construction Discipline Scientific Research Ability Promotion project (No. 2021ZDJS071), We also acknowledge the support of the Natural Science Foundation of Shaoguan University (No. SZ2020KJ03) and the innovation Projects of Colleges and Universities in Guangdong Province (No. 2021KTSCX122, 2022KQNCX077).

References

- J. Zhang, Z. Wang, T. Jiang, L. Xie, C. Sui, R. Ren, J. Qiao, K. Sun, "Densification of 8 mol% yttria-stabilized zirconia at low temperature by flash sintering technique for solid oxide fuel cells", *Ceram. Int.*, **43** (2017) 14037–14043.
- L. Guan, S. Le, S. He, X. Zhu, T. Liu, K. Sun, "Densification behavior and space charge blocking effect of Bi_2O_3 and Gd_2O_3 Co-doped CeO_2 as electrolyte for solid oxide fuel cells", *Electrochim. Acta*, **161** (2015) 129–136.
- M.I. Asghar, M. Heikkilä, P.D. Lund, "Advanced low-temperature ceramic nanocomposite fuel cells using ultra high ionic conductivity electrolytes synthesized through freeze-dried method and solid-route", *Mater. Today Energy*, **5** (2017) 338–346.
- A. Rafique, M.A. Ahmad, I. Shakir, A. Ali, G. Abbas, M.S. Javed, M.A. Khan, R. Raza, "Multioxide phase-based nanocomposite electrolyte (M@SDC where $\text{M} = \text{Zn}^{2+}/\text{Ba}^{2+}/\text{La}^{3+}/\text{Zr}^{2+}/\text{Al}^{3+}$) materials", *Ceram. Int.*, **46** (2020) 6882–6888.
- A.S. Kumar, R. Balaji, S. Jayakumar, C. Pradeep, "Microwave assisted sintering of gadolinium doped barium cerate electrolyte for intermediate temperature solid oxide fuel cells", *Mater. Chem. Phys.*, **182** (2016) 520–525.
- J. Zhang, C. Lenser, N.H. Menzler, O. Guillon, "Comparison of solid oxide fuel cell (SOFC) electrolyte materials for operation at 500°C ", *Solid State Ionics*, **344** (2020) 115138–115147.
- S. Chang, Z. Huang, C. Chen, H. Lei, S. Chen, Y. Jiang, "Preparation of zinc and alkaline earth metal co-doped apatite-type lanthanum silicate electrolyte ceramics by combustion method and mechanism of co-doping enhanced conductivity", *Ceram. Int.*, **46** [15] (2020) 24661–24667.
- Y. Zhao, L. Dai, Z. He, L. Wang, J. Cao, "Synthesis and characterization of Ba^{2+} and W^{6+} co-doped apatite-type lanthanum silicate electrolytes", *Ceram. Int.*, **46** [4] (2020) 5420–5429.
- L. Wang, C. Li, K. Ma, S. Zhang, G. Yang, C. Li, " $\text{La}_{0.8}\text{Sr}_{0.2}\text{Ga}_{0.8}\text{Mg}_{0.2}\text{O}_3$ electrolytes prepared by vacuum cold spray under heated gas for improved performance of SOFCs", *Ceram. Int.*, **44** [12] (2018) 13773–13781.
- K. Hwang, M. Jang, M. Kyu Kim, S. Hee Lee, T. Ho Shin, "Effective buffer layer thickness of La-doped CeO_2 for high durability and performance on $\text{La}_{0.9}\text{Sr}_{0.1}\text{Ga}_{0.8}\text{Mg}_{0.2}\text{O}_{3-\delta}$ electrolyte supported type solid oxide fuel cells", *J. Eur. Ceram. Soc.*, **41** [4] (2021) 2674–2681.
- P. Lacorre, F. Goutenoire, O. Bohnke, R. Retoux, Y. Laligant, "Designing fast oxide-ion conductors based on $\text{La}_2\text{Mo}_2\text{O}_9$ ", *Nature*, **404** [6780] (2000) 856–858.
- A. Das, I. Shajahan, H.P. Dasari, M.B. Saidutta, H. Dasari, "Dilatometer studies on LAMOX based electrolyte materials for solid oxide fuel cells", *Mater. Chem. Phys.*, **258** (2021) 123958–123965.
- S. Siddharth, A. Sil, "X-ray photo electron spectroscopy and ion dynamics study of W^{6+} doped $\text{La}_2\text{Mo}_2\text{O}_9$ as SOFC electrolyte", *Mater. Res. Bull.*, **105** (2018) 36–44.
- T. Saradha, A. Subramania, K. Balakrishnan, S. Muzhuthi, "Microwave-assisted combustion synthesis of nanocrystalline Sm-doped $\text{La}_2\text{Mo}_2\text{O}_9$ oxide-ion conductors for SOFC application", *Mater. Res. Bull.*, **68** (2015) 320–325.
- C. Tian, L. Shao, D. Ji, J. Yang, J. Xie, Q. Yin, H. Le, "Synthesis and characterization of tungsten and barium co-doped $\text{La}_2\text{Mo}_2\text{O}_9$ by sol-gel process for solid oxide fuel cells", *J. Rare Earths*, **37** [9] (2019) 984–988.
- H. Liu, J. Zhang, Z. Wen, J. Han, "Synthesis, sinterability, conductivity and reducibility of K^+ and W^{6+} double doped $\text{La}_2\text{Mo}_2\text{O}_9$ ", *Solid State Ionics*, **276** (2015) 90–97.
- D. Marrero-López, J. Peña-Martínez, J.C. Ruiz-Morales, D. Pérez-Coll, M.C. Martín-Sedeño, P. Núñez, "Applicability of $\text{La}_2\text{Mo}_{2-y}\text{W}_y\text{O}_9$ materials as solid electrolyte for SOFCs", *Solid State Ionics*, **178** [23–24] (2007) 1366–1378.
- R.N. Nayyar, S. Anwane, V. Gaikwad, V. Sathe, S. Acharya, "Correlation of dynamical disorder and oxy-ion diffusion mechanism in a Dy, W co-doped $\text{La}_2\text{Mo}_2\text{O}_9$ system: an electrolyte for IT-SOFCs", *Dalton Trans.*, **49** [38] (2020) 13406–13419.
- A. Sil, S. Bysakh, "Effect of K doping on Mo^{6+} stability and ionic conductivity study in $\text{La}_2\text{Mo}_2\text{O}_9$ as oxide-ion conductor", *Mater. Res. Express*, **6** [5] (2019) 056203.
- D.M. Zhang, Z. Zhuang, X.P. Wang, Y.X. Gao, Q.F. Fang, "Electrical properties of $\text{La}_2\text{Mo}_2\text{O}_9/\text{Al}_2\text{O}_3$ nanocomposites fabricated by microwave sintering method", *J. Eur. Ce-*

- ram. Soc., **32** [12] (2012) 3239–3247.
21. H. Cheng, W. Hongen, L. Liang, L. Zhouguang, Q. Dong, “Facile synthesis of $\text{La}_2\text{Mo}_2\text{O}_9$ nanoparticles via an EDTA complexing approach”, *Rare Met.*, **27** [4] (2008) 340–344.
 22. C. Tian, Q. Yin, J. Xie, J. Yang, H. Sun, B. Ji, W. Bao, “Chemical synthesis and properties of $\text{La}_{1.9}\text{Ba}_{0.1}\text{Mo}_{1.9}\text{Mn}_{0.1}\text{O}_9$ as electrolyte for IT-SOFCs”, *J. Rare Earths*, **32** [5] (2014) 423–428.
 23. D. Marrero-López, J. Canales-Vázquez, J.C. Ruiz-Morales, A. Rodríguez, J. Irvine, P. Núñez, “Synthesis, sinterability and ionic conductivity of nanocrystalline $\text{La}_2\text{Mo}_2\text{O}_9$ powders”, *Solid State Ionics*, **176** [23–24] (2005) 1807–1816.
 24. B.S. Prakash, V.K.W. Grips, S.T. Aruna, “A single step solution combustion approach for preparing gadolinium doped ceria solid oxide fuel cell electrolyte material suitable for wet powder and plasma spraying processes”, *J. Power Sources*, **214** (2012) 358–364.
 25. R.K. Singh, P. Singh, “Electrical conductivity of barium substituted LSGM electrolyte materials for IT-SOFC”, *Solid State Ionics*, **262** (2014) 428–432.
 26. W. Sun, Y. Jiang, Wang Y, S. Fang, Z. Zhu, W. Liu, “A novel electronic current-blocked stable mixed ionic conductor for solid oxide fuel cells”, *J. Power Sources*, **196** [1] (2011) 62–68.
 27. K.C. Anjaneya, G.P. Nayaka, J. Manjanna, G. Govindaraj, K.N. Ganesha, “Studies on structural, morphological and electrical properties of $\text{Ce}_{0.8}\text{Ln}_{0.2}\text{O}_{2-\delta}$ ($\text{Ln} = \text{Y}^{3+}, \text{Gd}^{3+}, \text{Sm}^{3+}, \text{Nd}^{3+}$ and La^{3+}) solid solutions prepared by citrate complexation method”, *J. Alloys Compd.*, **585** (2014) 594–601.
 28. W. Raza, M.M. Haque, M. Muneer, T. Harada, M. Matsumura, “Synthesis, characterization and photocatalytic performance of visible light induced bismuth oxide nanoparticle”, *J. Alloys Compd.*, **648** (2015) 641–650.
 29. Y. Chen, X. Lu, Y. Ding, X. Liu, G. Meng, “Microwave assisted synthesis, sinterability and properties of Ca-Zn codoped LaCrO_3 as interconnect material for IT-SOFCs”, *J. Rare Earths*, **28** [1] (2010) 153–157.
 30. Y.C. Wu, Y.Y. Liao, “Effect of Ca^{2+} and Sr^{2+} doping on the microstructure and cell performance of samaria-doped ceria electrolytes used in solid oxide fuel cells”, *Int. J. Hydrogen Energy*, **41** [31] (2016) 13591–13602.
 31. J. Wang, X. Chen, S. Xie, L. Chen, Y. Wang, J. Meng, D. Zhou, “Bismuth tungstate/neodymium-doped ceria composite electrolyte for intermediate-temperature solid oxide fuel cell: Sintering aid and composite effect”, *J. Power Sources*, **428** (2019) 105–114.
 32. A.J. Saikia, D. Tripathy, G.T. Tado, A. Pandey, “Effect of V^{5+} substitution on structural and electrical properties of $\text{La}_2\text{Mo}_2\text{O}_9$ ”, *Physica B Condens. Mat.*, **570** (2019) 133–138.
 33. J. Yang, Z. Wen, Z. Gu, D. Yan, “Ionic conductivity and microstructure of solid electrolyte $\text{La}_2\text{Mo}_2\text{O}_9$ prepared by spark-plasma sintering”, *J. Eur. Ceram. Soc.*, **25** [14] (2005) 3315–3321.
 34. F. Goutenoire, O. Isnard, E. Suard, O. Bohnke, Y. Laligant, R. Retoux, P. Lacorre, “Structural and transport characteristics of the LAMOX family of fast oxide-ion conductors, based on lanthanum molybdenum oxide $\text{La}_2\text{Mo}_2\text{O}_9$ ”, *J. Mater. Chem.*, **11** (2001) 119–124.
 35. L.N. Borah, A. Pandey, “Effect of Sn-doping at Mo-site on the conductivity of $\text{La}_2\text{Mo}_2\text{O}_9$ series of compounds”, *Indian J. Phys.*, **84** [6] (2010) 699–704.
 36. G. Dönmez, V. Sarıboğa, T. Gürkaynak Altınçekiç, M.A.F. Öksüzömer, “Polyol synthesis and investigation of $\text{Ce}_{1-x}\text{RE}_x\text{O}_{2-x/2}$ ($\text{RE} = \text{Sm}, \text{Gd}, \text{Nd}, \text{La}, 0 \leq x \leq 0.25$) electrolytes for IT-SOFCs”, *J. Am. Ceram. Soc.*, **98** [2] (2015) 501–509.
 37. B. Yan, M. Li, J. Zhang, K.C. Chou, “Structural and electrical properties of $\text{La}_{2-x}\text{Ba}_x\text{Mo}_2\text{O}_{9-x/2}$ ($x = 0-0.18$)”, *Mater. Res. Bul.*, **45** (2010) 382–387.